



In this study we investigated the distribution of the radiolabeled antibody within tumors at different time points up to 7 d after injection in relation to histology, antigen expression, and vascularization. We also calculated the intratumoral absorbed-dose rate distribution at the time of sacrifice in relation to the same factors.

## MATERIALS AND METHODS

### mAb

The chimeric (mouse/human) IgG1 mAb BR96 (Seattle Genetics Inc.) binds to the tumor-associated antigen Le<sup>y</sup>. Several human carcinoma types express Le<sup>y</sup>, including breast, gastrointestinal tract, pancreas, non-small cell lung, cervical, and ovarian cancers. BR96 also binds to some normal tissues, mainly epithelial cells of the gastrointestinal tract (23). The dissociation constant ( $K_d$ ) is 4 nM (22).

### Radioimmunoconjugate

BR96 was conjugated with the DOTA chelate (*S*-2-(4-isothiocyanatobenzyl)-1,4,7,10-tetraazacyclododecane tetraacetic acid; Macrocylics) as previously described (22). The number of DOTA moieties per BR96 molecule was determined by matrix-assisted laser desorption ionization mass spectroscopy. The antigen-binding properties (immuno-reactivity) of DOTA-BR96 relative to BR96 were determined by saturation binding curve analysis, using BN7005 cells as the target antigen. The immunoreactivity is given by the ratio  $K_d$  (BR96)/ $K_d$  (DOTA-BR96).

The following procedure was used for labeling with  $^{177}\text{LuCl}_3$  (MDS Nordion). Both the DOTA-BR96 conjugate in 0.25 M ammonium acetate buffer and the radionuclide solution were preheated at 45°C for 10 min. The DOTA-BR96 solution was then added to the radionuclide-containing vial and incubated at 45°C for 15 min. The reaction was quenched with an excess of diethylenetriaminepentaacetic acid for 5 min and diluted in 1% human serum albumin (Baxter Medical AB). The radiochemical purity of the labeled immunoconjugate was determined by instant thin-layer chromatography using a 1 × 9 cm silica-gel-impregnated fiberglass sheet, eluted in 0.1 M ethylenediamine tetraacetic acid. Separation by size-exclusion chromatography together with high-performance liquid chromatography (7.8 × 300 mm molecular sieving column, SEC S3000 [Phenomenex], eluted in 0.05 M sodium phosphate at 1.0 mL/min) was used to determine the radiochemical purity and to detect signs of aggregation or fragmentation.

### Rat Tumor Model

Immunocompetent male Brown Norway (BN) rats ( $n = 38$  for the main study; Harlan) with a mean body weight of 214 g (SD, 24 g) at the time of tumor cell inoculation were used. These animals express BR96-binding antigen in some normal tissues, mainly in the epithelium of the gastrointestinal tract (24). The animals were housed under standard conditions with standard pellets and fresh water ad libitum. All experiments were conducted in compliance with Swedish legislation on animal protection and were approved by the regional ethics committee on animal experiments.

BN7005-H<sub>1</sub>D<sub>2</sub> is a rat colon carcinoma cell line established from a 1,2-dimethylhydrazine-induced tumor from a Brown Norway rat. We have found that the fraction surviving 2 Gy at a high absorbed-dose rate

in vitro is 0.5 for this cell line. The cells were cultured in RPMI-1640 medium with stable glutamine supplemented with 10% fetal bovine serum (both from PAA Laboratories GmbH), 1 mM sodium pyruvate, 10 mM *N*-(2-hydroxyethyl)piperazine-*N'*-(2-ethanesulfonic acid) buffer, and a 14 µg/mL solution of gentamicin (all from Gibco Invitrogen) at 37°C, in a humidified environment containing 5% CO<sub>2</sub>. The cells were washed with phosphate-buffered saline, detached by trypsin treatment, and resuspended in supplemented medium. The animals were inoculated between the peritoneum and the abdominal wall with 3 × 10<sup>5</sup> cells under anesthesia (isoflurane; Abbott Scandinavia AB).

### Study Design and Biodistribution

The main study was conducted as 2 separate experiments referred to as group 1 and group 2 (Table 1). The tumors were measured, and their volumes were calculated as length × width<sup>2</sup> × 0.4, as previously established (25), at injection of the radioimmunoconjugate and at 72–168 h after injection. At 13–14 d after inoculation, 150 µg of  $^{177}\text{Lu}$ -DOTA-BR96 (in 0.4 mL of phosphate-buffered saline with 1% human serum albumin) were injected via a tail vein. The administered activity of  $^{177}\text{Lu}$ -DOTA-BR96 was 50 MBq/kg of body weight in group 1 and 25 MBq/kg in group 2. A lower activity was administered to group 2 to reduce possible radiation-induced cytotoxic effects in the tumors, and samples were taken at different time points to observe changes in activity distribution. Arterial blood samples were drawn 2 min after injection and before sacrifice for activity measurements in a NaI(Tl) well counter (group 1: 1282 Compugamma CS [LKB Wallac]; group 2: Wallac Wizard 1480 [PerkinElmer]). The animals were euthanized 2, 8, 24, 48, 72, 96, 120, and 168 h after injection, and the tumors were excised and cut in half. One half was embedded in Tissue-Tek O.C.T. compound (Sakura Finetek) and frozen on dry ice, and the activity of the other half was measured in a NaI(Tl) well counter. The frozen samples were cryosectioned, starting at the tumor center. Sections used for autoradiography were 20 µm (group 1) or 30 µm (group 2) thick. Sections used for staining were 10 µm thick and stored at –80°C.

[Table 1]

### Control of Antibody Effects

To evaluate untreated tumor histology and antigen expression and the therapeutic effects of the unlabeled antibody, 18 rats were inoculated with tumor cells as described above. Tumors from 9 untreated rats were excised on the day corresponding to antibody injection. The remaining 9 rats were injected with 0.1, 1.0, or 10.0 mg of unlabeled BR96 per kilogram ( $n = 3$ /group) and sacrificed 48 h after injection. The tumors were fixed in 4% paraformaldehyde and were embedded in paraffin before sectioning and staining for histology and antigen expression.

### Digital Autoradiography

The  $^{177}\text{Lu}$  activity distribution was imaged using microscope slides containing 3 tumor sections per slide. These were imaged for 10 h each, using a double-sided silicon strip detector with an intrinsic spatial resolution of 50 µm (Biomolex 700 imager; Biomolex AS). The recorded coordinates of all detected events were analyzed using IDL 6.4 software (ITT Visual Information Solutions). Corrections were applied for dead or miscalibrated strips and for radioactive decay.

**TABLE 1**  
Experimental Details for Two Animal Groups

Group	Injected activity (MBq/kg)	No. of animals sacrificed at each time point after injection							
		2 h	8 h	24 h	48 h	72 h	96 h	120 h	168 h
1	50	3	3	2	3	—	3	3	—
2	25	—	3	3	3	3	3	3	3

To determine the detector efficiency for each section thickness, adjacent tumor sections were imaged and their activity measured in the NaI(Tl) well counter for quantification of all tumor section images. The total mass of the sections on each slide was calculated by the section thickness times the density (1.0 g/cm<sup>3</sup>) times the area determined from histology stainings. Images were scaled to percentage injected activity per gram (%IA/g) using the mass, the total activity per section, and the decay-corrected injected activity. Visualization and region-of-interest (ROI)-based analysis of the images were performed using ImageJ software (26). Six ROIs (0.1–4.5 mm<sup>2</sup>) were drawn on 1 tumor section per animal, with 2 regions each outlining structures visually identified as having high, medium, and low levels of activity uptake relative to the entire section.

### Dosimetry

To calculate the absorbed-dose rate distribution in tumor sections at the time of sacrifice, a point-dose kernel (27) for <sup>177</sup>Lu was generated with the Monte Carlo code MCNP5 1.4 (28) using the new electron transport logic (dbn 17j 2). The point-dose kernel was modeled as concentric spheres with radii increasing in steps of 100 μm inside a 2.1-mm-diameter cube in a tissue-equivalent medium (1.00 g/cm<sup>3</sup>). Simulations included β-particles, γ-rays, conversion electrons, and Auger electrons emitted at the origin, with the energy deposition tallied in each layer. One imaged section per tumor was used. Each image was normalized to the activity at the time of sacrifice and stacked to form a new 3-dimensional dataset with the shortest diameter matching that of the point-dose kernel. The volume was down-sampled to cubic voxels with 100-μm sides before convolution with the point-dose kernel. The resulting absorbed-dose rate image was then extracted from the middle of the stack. Mean absorbed-dose rate for the whole section and in ROIs corresponding to those in the activity image were quantified.

### Histology and Immunohistochemistry

After autoradiography, the sections used for detection and adjacent sections were stained with Mayer hematoxylin and chromotrope 2R (both from Histolab AB). Sections were stained for the detection of antigen expression (BR96), blood vessel distribution (RECA-1; Abcam plc), and proliferation (anti-Ki67 clone SP6; Thermo Fisher Scientific Inc.). The slides were dried for 15 min at 37°C and then fixed either for 8 min with 4% phosphate-buffered formalin (Histolab AB, for antigen and proliferation staining) or for 5 min in ice-cold acetone (for staining of blood vessels). The sections were then washed with Tris-buffered saline with polysorbate 20, pH 7.4, and endogenous peroxidases were blocked by peroxidase-blocking solution (Dako) before the addition of primary antibodies. All antibodies were diluted in antibody diluent (Dako). The slides were incubated with the primary antibodies either overnight (BR96 and RECA-1) or for 2 h (SP6) in a moist chamber at room temperature. After washing, secondary antibodies were added to the slides. The secondary antibodies used were peroxidase-conjugated donkey antihuman IgG for the detection of BR96, peroxidase-conjugated donkey antimouse IgG for the detection of RECA-1, and peroxidase-conjugated donkey antirabbit IgG for the detection of SP6 (all from Jackson ImmunoResearch Laboratories Inc.). The slides were incubated for either 3 h (BR96 and RECA-1) or 1 h (SP6) in a moist chamber at room temperature. After washing, diaminobenzidine (Dako) was added before hematoxylin staining (1 min) and subsequent dehydration and mounting.

Areas corresponding to the ROIs were exported as individual images from adjacent sections stained for the detection of antigen expression and were processed to suppress blue cell nuclei staining. The ratio of stained to nonstained areas in each image was then calculated using ImageScope software (Aperio Technologies) and the Positive Pixel Count algorithm, version 9. Algorithm parameters were

calibrated separately per group of animals because of different staining intensities (Supplemental Fig. 1, available online at <http://jnm.snmjournals.org>).

### Statistical Analysis

To test the image quantification, the values of the mean %IA/g obtained from the digital autoradiography images were compared with the corresponding values from NaI(Tl) well counter measurements for the same tumors using a paired-samples *t* test. The activities measured by well counter for animal groups 1 and 2 were also compared at each time point after injection, using the nonparametric independent-samples Mann–Whitney *U* test. The Pearson correlation between the antigen staining ratio and the activity uptake, as well as the estimated absorbed-dose rate in the ROIs, was calculated at each time point that had data from at least 5 animals, that is, 30 ROIs. Normal distribution was assumed in this test because of the number of samples. All analyses were performed with IBM SPSS Statistics, version 19 (SPSS Inc.), with a *P* value of less than 0.05 being considered significant.

## RESULTS

### Radioimmunoconjugation

The mean number of DOTA molecules per IgG was determined to be 2.4. The immunoreactivity was given by the ratio of the K<sub>d</sub> for BR96 and DOTA-BR96 and was found to be 0.86, which was not significantly different from unlabeled BR96. The specific activity used for group 1 was 86 MBq/mg, the radiochemical purity according to instant thin-layer chromatography was more than 99%, and no aggregates or fragments were observed with high-performance liquid chromatography. The specific activity used for group 2 was 42.5 MBq/mg, the radiochemical purity was more than 97.5%, and there was a 1.3% labeled aggregated fraction according to high-performance liquid chromatography.

### Biodistribution

Biodistribution data for blood and tumors are presented in Table 2. Pharmacokinetic analysis of the decay-corrected %IA/g for blood resulted in an α-half-life of 5.6 h and a β-half-life of 32.5 h (nonlinear regression, 2-phase decay, GraphPad Prism 5.04). The mean tumor volume at injection was 650 mm<sup>3</sup> (SD, 235 mm<sup>3</sup>), and the median tumor uptake was 8.4 %IA/g (range 6.3–9.8 %IA/g) at 48 h after injection, after which there were increased variations in uptake and tumor volumes. Of the 18 tumors excised at 72 h or later, 3 had continued to grow, 4 had undergone minor

**TABLE 2**  
Activity of <sup>177</sup>Lu-DOTA-BR96 in Tumor and Blood

Time after injection (h)	<sup>177</sup> Lu-DOTA-BR96 activity (%IA/g)	
	Tumor	Blood
0	—	6.72 (5.82–8.70)
2	1.97 (1.54–2.13)	—
8	4.37 (3.15–6.38)	4.29 (4.13–4.62)
24	6.95 (5.09–10.2)	2.81 (2.52–2.94)
48	8.43 (6.34–9.81)	2.12 (1.95–2.43)
72	14.9 (7.48–19.0)	1.81 (1.37–1.99)
96	10.6 (4.24–20.7)	1.45 (1.29–1.89)
120	7.80 (2.65–13.0)	1.56 (1.45–1.64)
168	28.3 (11.6–52.1)	1.17 (0.98–1.69)

Data are median, followed by range in parentheses.

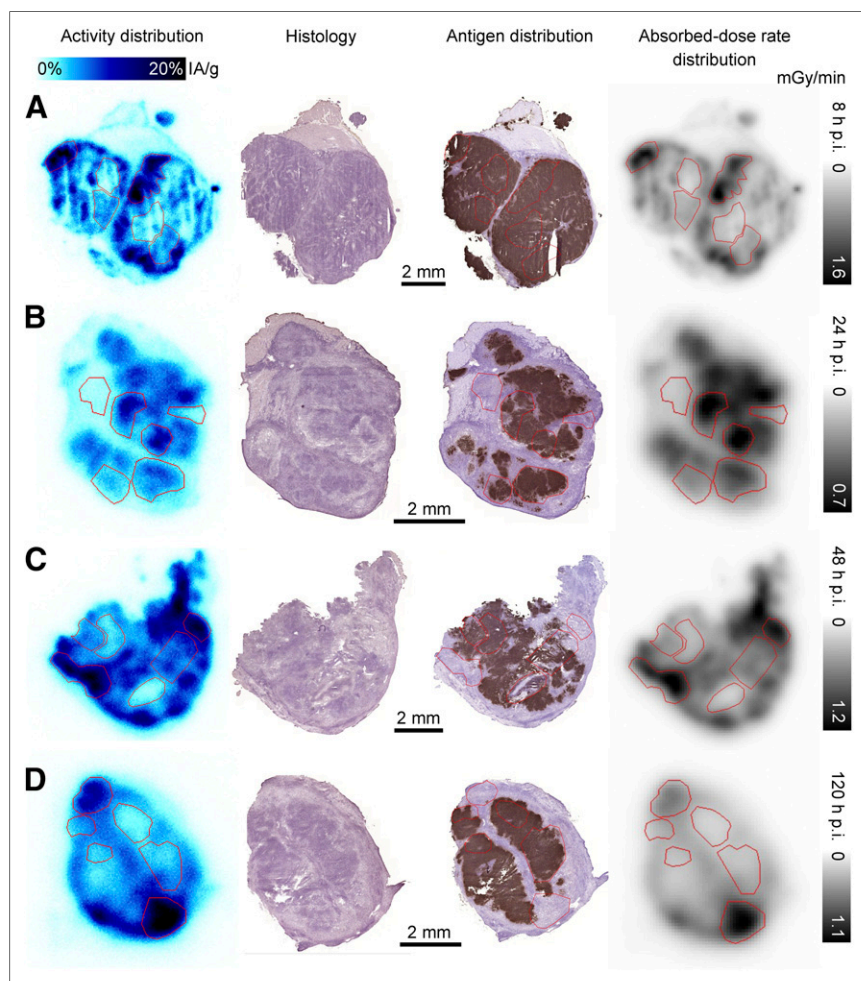
changes in volume, and 11 had decreased in size. No statistically significant difference in tumor %IA/g could be found between the 2 groups of animals at any time point after injection using a non-parametric test. No significant difference that would indicate a systematic error in image quantification was found between tumor activity uptake measured by well counter or by quantitative autoradiography.

#### Absorbed-Dose Rate at Moment of Sacrifice

Images of the absorbed-dose rate distributions were produced from digital autoradiography images. The intratumoral absorbed-dose rate distribution closely mimics the activity distribution (Fig. 1) because most of the energy is deposited close to the point of decay. Table 3 shows the median values and ranges for the mean absorbed-dose rate over the entire section presented for each time point and animal group.

[Fig. 1]

[Table 3]



RGB

**FIGURE 1.** Representative tumor sections from group 2 at 4 time points after injection. From left to right: digital autoradiography images of  $^{177}\text{Lu}$  distribution scaled to %IA/g, adjacent sections stained with hematoxylin and eosin for histologic examination, adjacent sections stained with BR96 antibody to determine antigen distribution, and absorbed-dose rate distribution at time of sacrifice based on activity image (individually scaled). ROIs used in correlation analysis are outlined in red where applicable. Sections from group 2 are displayed due to visually better-quality staining for antigen distribution. Peripheral distribution of activity in each nodule is shown at 8 h after injection (A), and correlation between uptake and antigen is shown at 24 h after injection (B). At 48 h after injection (C), this correlation has given way to correlation between activity and antigen-negative granulation tissue, which is even more pronounced at 120 h after injection (D). p.i. = after injection.

#### Activity Distribution in Comparison to Tumor Histology, Antigen Expression, and Vascularization

At 2 and 8 h after injection, the radioactivity was mainly distributed close to viable and antigen-positive tumor margins (Fig. 1A). The stainings showed dense tumor growth with necrotic areas at the center of the tumors. All tumors were well vascularized and contained a high proportion of proliferating cells, and the Le $\gamma$  antigen was detectable on almost all viable tumor cells. At 24 h after injection, the activity had penetrated the more central areas of the tumor sections; however, higher levels were still observed peripherally in half the evaluated tumors. The areas with high activity correlated mainly with antigen-positive areas in the viable regions (Fig. 1B). Tumors were well vascularized, and some also had small areas of granulation tissue. At 48 h after injection, there was a change in histology compared with untreated controls (Figs. [Fig. 2]

[Fig. 2]

2A and 2B), with areas of granulation tissue that overlapped activity hot spots in 5 of 6 tumors (Fig. 1C). Areas with low activity had high levels of available antigen, and blood vessels were detected in all areas. At 72–168 h after injection, the activity distribution varied among the individual tumors, ranging from local areas of high activity to a more homogeneous distribution. Tumors that decreased in size after the mAb injection contained few blood vessels and few proliferative cells, whereas the opposite was observed for tumors that continued to grow. Smaller tumors had fewer antigen-positive cells and a larger proportion of stroma or granulation tissue, often with high activity uptake, whereas larger tumors had dense areas of tumor cells and intense staining of the antigen, typically with limited uptake (Fig. 1D). There was no notable uptake in the necrotic areas over the time observed.

#### Control of Antibody Effects

Tumor cells from untreated animals all had complete membrane staining for the Le $\gamma$  antigen (Fig. 2B). The low BR96 dose of 0.1 mg/kg resulted in small areas of unstained tumor cells close to the tumor margins. Both 1.0 and 10.0 mg/kg led to limited antigen staining and altered histology, including the formation of granulation tissue and necrosis, whereas untreated and low-dose animals all showed dense growth of tumor cells with occasional areas of necrosis (Fig. 2).

#### ROI Analysis

The mean activity per gram, the mean absorbed-dose rate at the time of sacrifice, and the percentage of the area staining as antigen-positive were calculated for each ROI. The absorbed-dose rate in the high-uptake regions (Table 3) was approximately twice as high as the mean absorbed-dose rate for the whole section. The results of the Pearson correlation analysis for relationships between activity uptake and absorbed-dose

**TABLE 3**  
Estimated Absorbed-Dose Rates for Whole Tumor Sections and High- and Low-Uptake Regions (Relative to Each Section)

Time after injection (h)	Mean absorbed-dose (mGy/min)					
	Whole tumor sections		High-uptake ROIs		Low-uptake ROIs	
	Group 1	Group 2	Group 1	Group 2	Group 1	Group 2
2	0.10 (0.10–0.20)	—	0.40 (0.30–0.50)	—	0.10 (0.00–0.10)	—
8	0.37 (0.27–0.43)	0.49 (0.40–0.52)	0.67 (0.61–1.13)	1.01 (0.70–1.31)	0.18 (0.15–0.30)	0.27 (0.15–0.37)
24	(0.54–0.79)	0.48 (0.33–0.58)	1.12 (1.09–1.81)	0.81 (0.59–1.08)	0.47 (0.14–0.51)	0.25 (0.17–0.52)
48	0.60 (0.49–0.65)	0.53 (0.46–0.60)	1.06 (0.78–1.35)	0.90 (0.56–1.15)	0.33 (0.21–0.67)	0.28 (0.22–0.51)
72	—	0.71 (0.29–0.84)	—	1.43 (0.51–1.65)	—	0.27 (0.17–0.77)
96	0.43 (0.25–1.04)	0.39 (0.38–0.63)	0.78 (0.48–1.03)	0.93 (0.70–1.17)	0.23 (0.18–0.35)	0.35 (0.19–0.53)
120	0.38 (0.30–0.66)	0.37 (0.34–1.88)	0.78 (0.56–1.43)	0.79 (0.45–3.62)	0.23 (0.17–0.34)	0.29 (0.17–2.92)
168	—	1.10 (0.76–2.40)	—	1.73 (1.23–5.31)	—	0.52 (0.17–3.01)

Data are median, followed by range in parentheses.

**[Table 4]** rate, and the antigen-positive area, are given in Table 4. The correlation coefficient changed over time, from positive at 8 and 24 h after injection to negative from 48 h after injection onward (Fig. 3). **[Fig. 3]** Activity uptake and absorbed-dose rate exhibited similar correlations with antigen, though the correlation with absorbed-dose rate was stronger at earlier than at later time points.

#### DISCUSSION

The results of this study show the dynamic process of intratumoral antibody distribution in a syngeneic animal model and how

a heterogeneous distribution results in a considerable variation in the absorbed-dose rate. Initially, the activity was localized to the periphery of the tumor, presumably near perfused blood vessels, and then there was a comparatively homogeneous distribution corresponding to viable antigen-expressing tumor tissue at 24 h after injection. The subsequent trend toward an increasing correlation between activity uptake and granulation tissue was interpreted as the effect of treatment, reducing viable, antigen-positive tumor cells in areas with high activity uptake. Activity uptake does not necessarily infer antibody uptake, since it is not known whether the radionuclide was still coupled to the mAb or was free after degradation, or whether the mAb was intact or fragmented. The ROI-based analysis showed a negative correlation between antigen expression and activity uptake from 48 h after injection onward. This correlation was stronger than that reported previously by Flynn et al. (16), who based their results on a pixel-by-pixel correlation between CEA and antibody in a subcutaneous xenograft. Although the methods of analysis differ, differences in antigen expression, vascularization, and immune response between the animals used are also likely to have been a factor (17). The increased variance in tumor activity uptake after 48 h after injection was attributed to variations in tumor growth or reduction, as has been observed elsewhere (19). The new cell populations present in several tumors had little activity uptake, probably because of a lower antibody concentration in the blood. This increased variance is likely more evident in syngeneic animal tumor models, which often show a faster rate of proliferation than do human tumors (21). No correlation was apparent between individual tumor growth or reduction and intratumoral activity distribution in this study.

Starting at 24 h after injection, the histologic properties of the tumors changed from predominantly proliferative tumor cells to areas of granulation tissue, concurrent with a decrease in tumor volumes. To allow the mAb distribution to be studied separately from radiotherapeutic effects, the administered activities were kept lower than those needed for clinical response according to our previous work (22). Therefore, these effects may be due to an immunologic response mediated via the Fc region of the antibodies (29,30), as is supported by the presence of granulation tissue in tumors from animals treated with unlabeled BR96 but not in untreated controls. At therapeutic activities of  $^{177}\text{Lu}$  (400 MBq/kg), the decrease in peripheral leukocytes (22) probably results in an

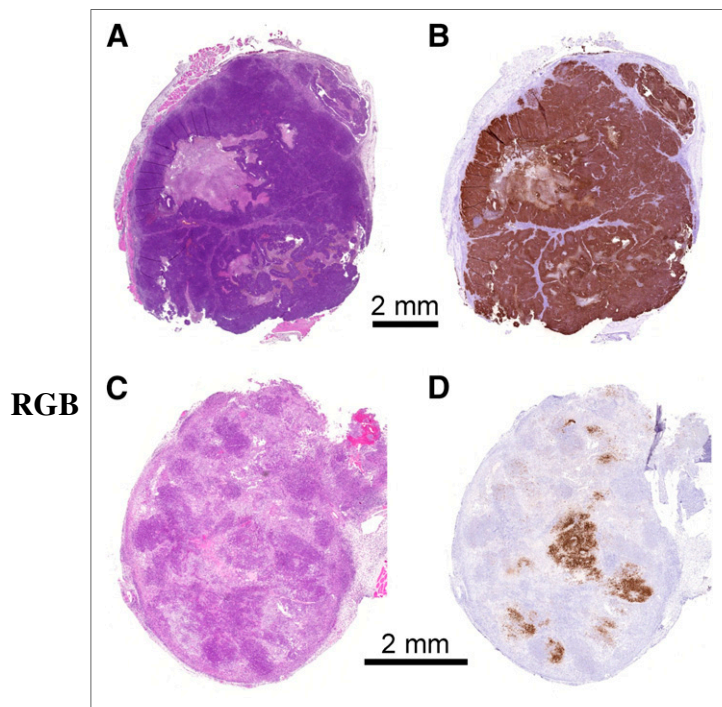


**FIGURE 2.** Representative tumor sections from untreated animals (top), and animals treated with 1.0 mg/kg dose of unlabeled mAb 48 h after injection (bottom). Sections are stained with hematoxylin and eosin (A and C) and BR96 antibody (B and D). Reduction in viable, antigen-expressing tumor cells is seen in tumor treated with unlabeled mAb.

**TABLE 4**  
Correlation Between Activity Uptake and Absorbed-Dose Rate at Time of Sacrifice vs. Antigen-Positive Area Fraction in ROIs of Tumor Sections

Time after injection(h)	Pearson correlation coefficient	
	Antigen vs. activity uptake	Antigen vs. absorbed-dose rate at time of sacrifice
8	0.450*	0.568 <sup>†</sup>
24	0.384*	0.405*
48	-0.432*	-0.490*
96	-0.711 <sup>†</sup>	-0.643 <sup>†</sup>
120	-0.621 <sup>†</sup>	-0.572 <sup>†</sup>

\* $P < 0.05$ .  
<sup>†</sup> $P < 0.001$ .

impaired immune response. Instead, with absorbed-dose rates and total absorbed doses approximately 8 times higher than in this study, radiation-induced cell death might dominate in achieving complete response (31).

Calculations of absorbed-dose rate distributions at different time points showed that high-uptake regions have twice the absorbed-dose rate of the whole tumor section mean. Estimating the accumulated mean absorbed doses to tumor over several days from the calculated absorbed-dose rates showed that they would fall into the area of several grays at late time points—absorbed doses leading to most cells dying if given at a single instant in an *in vitro* assay. However, the low <sup>177</sup>Lu activity and absorbed-dose rate in this study may allow the tumor to repair DNA damage and repopulate by proliferation of undamaged or restored cells. The correlation between viable, antigen-expressing tissue and areas of relatively high absorbed-dose rate at 24 h after injection indicates that using a longer-range  $\beta$ -emitter such as <sup>90</sup>Y would not necessarily increase tumor cell death at therapeutic activities. In contrast, the concentration of activity in areas of granulation tissue and stroma at later times suggests that a radionuclide with a shorter half-life than that used in the present study would be more bene-

ficial. Further studies, particularly at therapeutic activity levels, are needed to fully evaluate the effects of the intratumoral temporal activity distribution on the efficacy of radioimmunotherapy in relation to radionuclide half-life and emission properties.

Earlier studies using models of colorectal cancer in immunodeficient mice show limited agreement with our observations of activity accumulation in granulation and stromal tissue at later time points. Two studies have reported uptake of <sup>125</sup>I-labeled anti-CEA antibody in necrotic areas at 48 h after injection and onward, although this finding is most likely an effect of free antibody or iodine pooling in blood (16,19). Studies of anti-CEA antibodies in subcutaneous xenografts of well-differentiated and regularly vascularized tumors exhibited a similar pattern of uptake to that in our model, whereas the antibody never penetrated very far from the blood vessels in poorly differentiated and vascularized tumors (17). Observations of another antibody, A33, in a well-differentiated model also showed early uptake around blood vessels resulting in homogeneous tumor uptake by 48 h after injection (15). Anti-CEA antibodies had penetrated well-vascularized intrahepatic xenografts effectively at 24 h after injection (18–20), which is more in agreement with our results, compared with subcutaneous tumors of the same cell line (17,32). Lower-affinity antibodies (e.g., anti-HER2) penetrate tumors more efficiently (9), and modeling predicts that binding-site barrier effects are unlikely for mAbs with a  $K_d$  greater than 1 nM (33), such as BR96 ( $K_d = 4$  nM). The observed reduction in tumor cell density at around 24–48 h after injection could also affect the activity distribution since apoptosis-inducing pretreatment has been shown to increase the rate and extent of antibody penetration (12,34).

## CONCLUSION

The results of this study show that the initial process of antibody penetration into viable antigen-expressing tumor areas occurs over approximately 24 h and is followed by a decreasing association between activity uptake and viable, antigen-expressing tumor tissue over a period of several days. This finding indicates that delivering a high absorbed-dose rate during the initial penetration and uptake period is especially important for a therapeutic response.

## DISCLOSURE

The costs of publication of this article were defrayed in part by the payment of page charges. Therefore, and solely to indicate this fact, this article is hereby marked “advertisement” in accordance with 18 USC section 1734. This research was supported by grants from the Swedish Research Council, the Swedish Cancer Society, Mrs. Berta Kamprad’s Foundation, Gunnar Nilsson’s Foundation, the Crafoord Foundation, Government Funding of Clinical Research within the National Health Service, King Gustaf V’s Jubilee Foundation, the Lund University Medical Faculty Foundation, the Eurostars program through the Swedish Governmental Agency for Innovation Systems (VINNOVA), and the Lund University Hospital Fund. No other potential conflict of interest relevant to this article was reported.

## ACKNOWLEDGMENTS

We thank Dr. Erik Larsson (Medical Radiation Physics, Lund University) for simulating the point-dose kernel, Dr. Peter Senter (Seattle Genetics, Inc.) for kindly providing the BR96 mAb, and

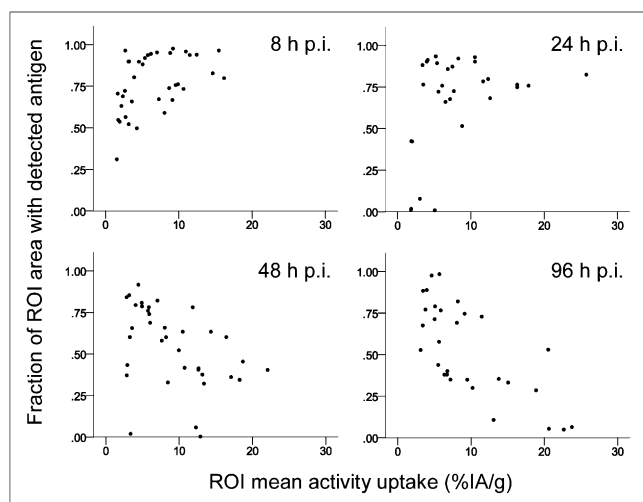


**FIGURE 3.** Scatter plots demonstrating changing correlation between antigen expression and activity over time. p.i. = after injection.

Dr. Otto Ljungberg (Department of Pathology, Skåne University Hospital, Malmö) for excellent help with histologic evaluations.

## REFERENCES

1. Jain M, Venkatraman G, Batra SK. Optimization of radioimmunotherapy of solid tumors: biological impediments and their modulation. *Clin Cancer Res.* 2007;13:1374–1382.
2. Huang CY, Pourgholami MH, Allen BJ. Optimizing radioimmunoconjugate delivery in the treatment of solid tumor. *Cancer Treat Rev.* 2012;38:854–860.
3. Minchinton AI, Tannock IF. Drug penetration in solid tumours. *Nat Rev Cancer.* 2006;6:583–592.
4. Beckman RA, Weiner LM, Davis HM. Antibody constructs in cancer therapy: protein engineering strategies to improve exposure in solid tumors. *Cancer.* 2007;109:170–179.
5. Tabrizi M, Bornstein GG, Suria H. Biodistribution mechanisms of therapeutic monoclonal antibodies in health and disease. *AAPS J.* 2010;12:33–43.
6. Netti PA, Berk DA, Swartz MA, Grodzinsky AJ, Jain RK. Role of extracellular matrix assembly in interstitial transport in solid tumors. *Cancer Res.* 2000;60:2497–2503.
7. Choi J, Credit K, Henderson K, et al. Intraperitoneal immunotherapy for metastatic ovarian carcinoma: resistance of intratumoral collagen to antibody penetration. *Clin Cancer Res.* 2006;12:1906–1912.
8. Fujimori K, Covell DG, Fletcher JE, Weinstein JN. A modeling analysis of monoclonal antibody percolation through tumors: a binding-site barrier. *J Nucl Med.* 1990;31:1191–1198.
9. Rudnick SI, Lou J, Shaller CC, et al. Influence of affinity and antigen internalization on the uptake and penetration of Anti-HER2 antibodies in solid tumors. *Cancer Res.* 2011;71:2250–2259.
10. Smith-Jones PM, Vallabhajosula S, Navarro V, Bastidas D, Goldsmith SJ, Bander NH. Radiolabeled monoclonal antibodies specific to the extracellular domain of prostate-specific membrane antigen: preclinical studies in nude mice bearing LNCaP human prostate tumor. *J Nucl Med.* 2003;44:610–617.
11. Ruggiero A, Holland JP, Hudolin T, et al. Targeting the internal epitope of prostate-specific membrane antigen with <sup>89</sup>Zr-7E11 immuno-PET. *J Nucl Med.* 2011;52:1608–1615.
12. Jang SH, Wientjes MG, Lu D, Au JL. Drug delivery and transport to solid tumors. *Pharm Res.* 2003;20:1337–1350.
13. Ferlay JSH, Bray F, Forman D, Mathers C, Parkin DM. GLOBOCAN 2008 v1.2, cancer incidence and mortality worldwide: IARC CancerBase no. 10. IARC Web site. <http://globocan.iarc.fr>. Accessed May 10, 2012.
14. Hess KR, Varadhachary GR, Taylor SH, et al. Metastatic patterns in adenocarcinoma. *Cancer.* 2006;106:1624–1633.
15. Antoniow P, Farnsworth AP, Turner A, et al. Radioimmunotherapy of colorectal carcinoma xenografts in nude mice with yttrium-90 A33 IgG and Tri-Fab (TFM). *Br J Cancer.* 1996;74:513–524.
16. Flynn AA, Boxer GM, Begent RH, Pedley RB. Relationship between tumour morphology, antigen and antibody distribution measured by fusion of digital phosphor and photographic images. *Cancer Immunol Immunother.* 2001;50:77–81.
17. El Emir E, Qureshi U, Dearling JL, et al. Predicting response to radioimmunotherapy from the tumor microenvironment of colorectal carcinomas. *Cancer Res.* 2007;67:11896–11905.
18. Fidarova EF, El-Emir E, Boxer GM, et al. Microdistribution of targeted, fluorescently labeled anti-carcinoembryonic antigen antibody in metastatic colorectal cancer: implications for radioimmunotherapy. *Clin Cancer Res.* 2008;14:2639–2646.
19. Dearling JL, Flynn AA, Qureshi U, et al. Localization of radiolabeled anti-CEA antibody in subcutaneous and intrahepatic colorectal xenografts: influence of tumor size and location within host organ on antibody uptake. *Nucl Med Biol.* 2009;36:883–894.
20. Frampas E, Maurel C, Remaud-Le Saec P, et al. Pretargeted radioimmunotherapy of colorectal cancer metastases: models and pharmacokinetics predict influence of the physical and radiochemical properties of the radionuclide. *Eur J Nucl Med Mol Imaging.* 2011;38:2153–2164.
21. Workman P, Aboagye EO, Balkwill F, et al. Guidelines for the welfare and use of animals in cancer research. *Br J Cancer.* 2010;102:1555–1577.
22. Eriksson SE, Ohlsson T, Nilsson R, Tennvall J. Repeated radioimmunotherapy with <sup>177</sup>Lu-DOTA-BR96 in a syngeneic rat colon carcinoma model. *Cancer Biother Radiopharm.* 2012;27:134–140.
23. Hellström I, Garrigues HJ, Garrigues U, Hellstrom KE. Highly tumor-reactive, internalizing, mouse monoclonal antibodies to Le(y)-related cell surface antigens. *Cancer Res.* 1990;50:2183–2190.
24. Sjögren HO, Isaksson M, Willner D, Hellström I, Hellström KE, Trail PA. Antitumor activity of carcinoma-reactive BR96-doxorubicin conjugate against human carcinomas in athymic mice and rats and syngeneic rat carcinomas in immunocompetent rats. *Cancer Res.* 1997;57:4530–4536.
25. Badn W, Kalliomaki S, Widegren B, Sjögren HO. Low-dose combretastatin A4 phosphate enhances the immune response of tumor hosts to experimental colon carcinoma. *Clin Cancer Res.* 2006;12:4714–4719.
26. Home page. IMAGEJ Web site. <http://imagej.nih.gov/ij/>. Accessed June 10, 2013.
27. Roeske JC, Aydogan B, Bardies M, Humm JL. Small-scale dosimetry: challenges and future directions. *Semin Nucl Med.* 2008;38:367–383.
28. X-5 Monte Carlo Team. *MCNP: A General Monte Carlo N-Particle Transport Code, Version 5. Vol I: overview and theory.* Los Alamos, NM: Los Alamos National Laboratory; 2003 (revised February 1, 2008). Report LA-UR-03-1987.
29. Ferris RL, Jaffee EM, Ferrone S. Tumor antigen-targeted, monoclonal antibody-based immunotherapy: clinical response, cellular immunity, and immunoescape. *J Clin Oncol.* 2010;28:4390–4399.
30. Houot R, Kohrt HE, Marabelle A, Levy R. Targeting immune effector cells to promote antibody-induced cytotoxicity in cancer immunotherapy. *Trends Immunol.* 2011;32:510–516.
31. Song H, Sgouros G. Radioimmunotherapy of solid tumors: searching for the right target. *Curr Drug Deliv.* 2011;8:26–44.
32. Rhoden JJ, Wittrup KD. Dose dependence of intratumoral perivascular distribution of monoclonal antibodies. *J Pharm Sci.* 2012;101:860–867.
33. Wittrup KD, Thurber GM, Schmidt MM, Rhoden JJ. Practical theoretic guidance for the design of tumor-targeting agents. *Methods Enzymol.* 2012;503:255–268.
34. Jang BS, Lee SM, Kim HS, et al. Combined-modality radioimmunotherapy: synergistic effect of paclitaxel and additive effect of bevacizumab. *Nucl Med Biol.* 2012;39:472–483.